Inverse modeling of pan heating in domestic cookers

F. Sanz-Serrano[a,*], C. Sagues[a], S. Llorente[b]

[a]*I3A Universidad de Zaragoza, Mariano Esquillor s/n, Zaragoza 50018, Spain*
[b]*Research and Development Department, Induction Technology, Product Division Cookers, BSH Home Appliances Group, Avenida de la Industria 49, Zaragoza 50016, Spain*

Abstract

The heating uniformity of the cooking vessels in domestic stoves depends on the type of heat source (induction, electric resistance, gas burner…) and of the way in which the power is transferred to the pan. The evaluation of the stoves functionalities is currently carried out by the manufacturers with costly experimental tests with real food, which are an important phase of the design process for the improvement of their performance in the food elaboration. In order to help to design the cookers and avoid the expensive tests, it is interesting to know how the heating power is distributed in each situation, so that the cookers can be adapted to obtain a more uniform heating. The contribution of this work is an inverse thermal model for the three aforementioned technologies of domestic cookers, which allows the calculation of the power distribution generated in the bottom of the pan from the measurement of the surface temperature. The results show that the proposed inverse model is of interest in many practical situations and can be used under diverse conditions.

Keywords: Domestic cooking; Thermal model; Inverse model; Power distribution.

1. Introduction

Domestic cooking appliances have significantly evolved during the last decades, not only those based in the traditional technology of gas burners, but also the newest cooking hobs with induction heating elements. The main

* Corresponding author. Tel.:+34-669-917-886.
E-mail addresses: fer.sanz@unizar.es (F. Sanz-Serrano), csagues@unizar.es (C. Sagues), sergio.llorente@bshg.com (S. Llorente).

improvements which have been introduced are related to the efficiency, the total heating power, and the number and configuration of the burners, inductors, hotplates, etc. In order to study the performance of the technologies and configurations of cookers, the manufacturers carry out different tests over their products, including cooking tests with real food, emulating a normal operation at the user's home. However, these tests imply spending time and money which could be saved with an appropriate modeling and simulation of the cooking processes. Moreover, with theoretical studies of different cooking situations (contact frying, deep-frying, boiling, etc.), a deeper understanding of the elaboration of the food could be reached, and the cooking stoves could be improved with better designs and functionalities.

Some authors in the current literature have studied the behavior of cooking stoves and pots with theoretical models or experimentation. Authors in [1] experimented with different technologies of stoves (gas, electric hotplate, induction) studying the performance in heating speed and temperature distribution in a pan frying process. Also in this context, the thermal efficiency of pots in a particular type of electric stove was calculated and measured in [2]. Further authors have developed different theoretical models of some cooking techniques, e.g. a thermal model of the elaboration of frozen hamburger patties was proposed in [3] and authors in [4] presented a model of the contact baking of thick pancakes. These models combine heat and mass transfer phenomena and include the food state variation as a result of the temperature rise. They are centered in the behavior of the food, and take into consideration that the heat source is well known and controlled, and that the temperature distribution in the pan is uniform. However, this assumption is far from a real cooking situation in a domestic environment, where the power distribution which determines the heating uniformity depends on the type of technology, the cooker design or the cooking vessel. In order to develop theoretical models closer to real scenarios and analyze the effects of the non-uniform heating on the elaboration of the food, it becomes of high interest to study the power distribution in the cooking vessels depending on the type of heat source.

In the particular case of induction cooktops, which is still a recent technology in the field of home appliances, there scarcely are previous works related to thermal modeling [5]. There can be found works in which the authors propose different methods to calculate the induced power distribution, generally using FEM software, which implicate elevated computational cost [6–8]. The power distribution transferred to the pans using gas range stoves or electric hotplates barely appears in the literature, even though they are the traditional technologies used in

worldwide kitchens.

In this work we propose an inverse model which allows the calculation of the power distribution generated in the bottom of the pan from the measurement of the top surface temperature. Different models are developed considering the most common heating technologies used in domestic cooktops. The inverse method has been used by other authors in thermal modeling for industrial applications [9–13], and it is particularly useful for the estimation of non-measurable variables, such as heat fluxes or heat transfer coefficients. In this work, for the temperature measurement we use an infrared camera, and the model is solved using a numerical method based in finite differences. In order to be able to use the infrared camera the cooking vessel must be empty, because the emissivity of the measured surface must be well known. Moreover the power distribution is considered independent of the content of the cooking vessel, thus it is not included in the proposed model.

2. Theory

The temperature reached inside a cooking vessel when it is heated in a domestic cooker is a consequence of the heating source and the way in which the power is transferred to the base of the pan. For example, in induction cookers this power distribution depends on the geometry of the coils, number of turns, distance between turns, etc. Thus, the design of the inductor can be optimized to obtain a uniform heating of the pans.

As stated in our previous work [5], the temperature evolution on each point of the base of a cooking vessel, placed over a heating source, obeys the heat equation:

$$P + \lambda \nabla^2 T = \rho C_p \frac{\partial T}{\partial t} \tag{1}$$

where P is the volumetric power density generated by the heating source. The second term is the heat flux of conduction, where $\nabla^2 T$ is the Laplacian of the temperature (T) and λ is the heat conductivity of the material. The term on the right is the variation of the energy stored in the system with time, where the material has density ρ and specific heat capacity C_p. The inverse modeling in this thermal problem consists in obtaining the value of the power density distribution in each point of the domain and each instant, from the temperature distribution measured during a heating process (for example with an infrared camera). The first step is to define the domain and state the boundary conditions of the problem, which are different depending on the heating source employed.

The most common cooking vessels in the world's market have a round shape. Therefore, we propose a model for a cylindrical geometry using polar coordinates (r, ϕ, z) with origin in the center of the base of the pan. Thus, the heat equation (1) can be expressed as:

$$P = -\lambda \left(\frac{1}{r}\frac{\partial T}{\partial r} + \frac{\partial^2 T}{\partial r^2} + \frac{1}{r^2}\frac{\partial^2 T}{\partial \phi^2} + \frac{\partial^2 T}{\partial z^2} \right) + \rho\, C_p \frac{\partial T}{\partial t} \,. \tag{2}$$

The inverse thermal model proposed allows the study of the power transfer with different configurations of inductors, and also for other common technologies, which are gas burners and electric stoves. It is valid for each one of the studied technologies. However, a different model with different domain and boundary conditions is considered for each case. The pan is modeled as a thin disk of homogeneous ferromagnetic material with known thermal properties and geometry, Fig. 1. The disk radius is R_p and its thickness is e_p. In the case of the induction hob and the electric stove, the steel disk is placed on a ceramic glass with thickness e_g, which also appears in the model. In the case of a gas cooker only the metallic disk is considered. Due to the complexity of the thermal problem, and the discrete nature of the input data (thermography), a numerical method based in finite differences is used to solve the inverse problem and compute the power distribution.

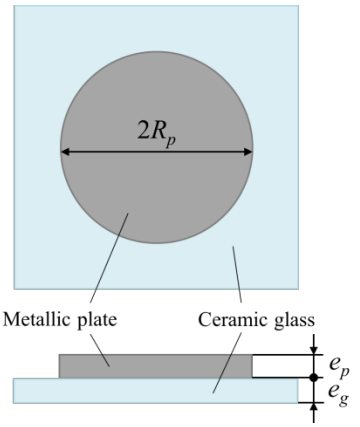

Fig. 1. Scheme of the plate which models the cooking vessel and the ceramic glass used in the induction hob and the electric stove to isolate the heating element from the user. In a gas cooker there is no glass beneath the disk.

2.1. Induction hob

In an induction hob a planar coil generates a current density J inside the base of a cooking vessel, which is made

of ferromagnetic material. This current is dissipated because of the Joule effect and generates a volumetric power density distribution P which heats the material

$$P = \frac{J^2}{\sigma e_p} \tag{3}$$

where σ is the electrical conductivity of the material and e_p is the pan base thickness. There is also an additional heat generated by the hysteresis effect, which is usually negligible. In most induction hobs the pan is placed over a ceramic glass which electrically isolates the inductor from the user (Fig. 2). The heat generated in the pan is transferred by conduction to the glass through a thermal contact conductance h_C, which includes the imperfect contact between both surfaces due to the intrinsic rugosity of the materials. Losses to the environment in the top surface of the pan base, the disk border and the glass are due to convection and radiation (h_p , h_b , h_g) .

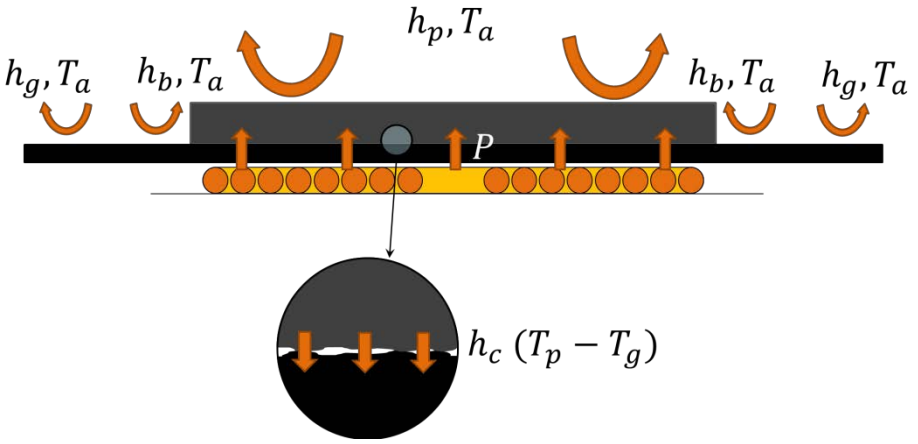

Fig. 2. Scheme of the thermal model in an induction hob. The coil generates a magnetic field which induces an eddy current density which is dissipated in the metallic material, resulting in the power distribution P. The heat is transferred from the pan by conduction to the glass, through a contact conductance factor h_c. The temperature of the metallic plate and the glass are T_p and T_g. The losses to the environment at temperature T_a, from the pan and the glass, are modeled with heat transfer coefficients h_p, h_g , which include convection and radiation. The losses in the perimeter of the pan base are modeled with a different heat transfer coefficient h_b, which can also model the effect of the walls of the pan.

As aforementioned, in the proposed model the pan base is modeled as a disk with radius R_p and thickness $e_p$of homogeneous material with known conductivity, density and heat capacity ($\lambda_p, \rho_p, C_{p_p}$) . A cylindrical area of the

glass with radius R_g and thickness e_g, being $R_g \geq R_p$, is also considered, with known properties ($\lambda_g, \rho_g, C_{p_g}$). The boundary conditions imposed in this model are Neumann boundary conditions [14]. In the top surface of the plate it is considered that the heat flux in z direction is equal to the losses to the environment due to convection and radiation:

$$-\lambda_p \frac{\partial T_p}{\partial z} = h_p \left(T_p - T_a\right)\Big|_{z=e_p, 0 \leq r \leq R_p} \tag{4}$$

$$h_p = h_{p_{conv}} + h_{p_{rad}} = h_{p_{conv}} + \sigma\varepsilon \left(T_p^2 + T_a^2\right)\left(T_p + T_a\right) \tag{5}$$

where T_p is the plate temperature, T_a is the ambient temperature, $h_{p_{conv}}$ is the convection coefficient on the plate, σ is the Stefan Boltzmann constant and $\varepsilon = 1$ is the emissivity considering that the radiant surface behaves as a black body and that the surrounding surfaces are at the ambient temperature. A similar condition is set on the top surface of the glass, in the outer area which is not in contact with the disk:

$$-\lambda_g \frac{\partial T_g}{\partial z} = h_g \left(T_g - T_a\right)\Big|_{z=0, R_p \leq r \leq R_g} \tag{6}$$

$$h_g = h_{g_{conv}} + h_{g_{rad}} = h_{g_{conv}} + \sigma\varepsilon \left(T_g^2 + T_a^2\right)\left(T_g + T_a\right) \tag{7}$$

where T_g is the glass temperature and $h_{g_{conv}}$ is the convection coefficient on the glass. For simplicity, in this work we consider that the convection coefficients are constant with the temperature, as the range of temperature in a pan in a domestic cooker is relatively small. In the bottom surface of the plate the vertical heat flux depends on the contact conductance h_c and the temperature of the glass, and it is identical to the heat flux in the top surface of the glass:

$$-\lambda_p \frac{\partial T_p}{\partial z} = -\lambda_g \frac{\partial T_g}{\partial z} = h_c \left(T_g - T_p\right)\Big|_{z=0} . \tag{8}$$

The vertical heat flux in the bottom surface of the glass is considered negligible for simplicity

$$-\lambda_g \frac{\partial T_g}{\partial z} = 0\Big|_{z=-e_g} . \tag{9}$$

In the radial direction, it is considered that the heat flux in the center is null, in both the plate and the glass, due to the symmetry of the problem. In the border of the plate a heat losses coefficient h_b is defined, which includes convection and radiation:

$$-\lambda_p \frac{\partial T_p}{\partial r} = -\lambda_g \frac{\partial T_g}{\partial r} = 0\Big|_{r=0} \tag{10}$$

$$-\lambda_p \frac{\partial T_p}{\partial r} = h_b \left(T_p - T_a\right)\Big|_{r=R_p} . \tag{11}$$

Finally, a Dirichlet boundary condition is considered in the border of the domain which models the glass

$$T_g = T_a\big|_{r=R_g}. \tag{12}$$

In order to solve the model a finite differences method is proposed [15]. The disk and the cylindrical volume of glass are discretized with the two-dimensional polar grid shown in Fig. 3. The position of each element is defined with R_i, ϕ_j, and the size of each grid element is $\Delta R, \Delta\phi$. The domain is not discretized in z direction because the heat conduction inside the plate and the glass is considered unimportant in this dimension due to the small thickness. The size of the time step selected in the discretization of the temporal dimension is Δt. The proposed method is an implicit finite differences method, in which the second derivatives of the temperature are approximated with a central differences scheme, and the first derivatives are approximated with a regressive differences scheme. Thus, the stability and convergence of the method are ensured. The power distribution in each element $P_{i,j}$ for each instant is related with the disk temperature measured in each element $T_{p_{i,j}}$ and the glass temperature $T_{g_{i,j}}$ with the expressions:

$(1 \leq i \leq n,\ \ 1 \leq j \leq M)$

$$P_{i,j} = a_{p_i} T_{p_{i,j}} + b^{+}_{p\,i} T_{p_{i+1,j}} + b^{-}_{p\,i} T_{p_{i-1,j}} + c_{p_i} T_{p_{i,j+1}} + c_{p_i} T_{p_{i,j-1}} - \frac{\rho_p C_{p_p}}{\Delta t} T^{\tau}_{p\,i,j} - a^{*}_{p_i} T_a - d_{p_i} T_{g_{i,j}} \quad (13)$$

$$(1 \le i \le N,\ \ 1 \le j \le M)$$

$$0 = a_{g_i} T_{g_{i,j}} + b^{+}_{g\,i} T_{g_{i+1,j}} + b^{-}_{g\,i} T_{g_{i-1,j}} + c_{g_i} T_{g_{i,j+1}} + c_{g_i} T_{g_{i,j-1}} - \frac{\rho_g C_{p_g}}{\Delta t} T^{\tau}_{g\,i,j} - a^{*}_{g_i} T_a - d_{g_i} T_{p_{i,j}} \quad (14)$$

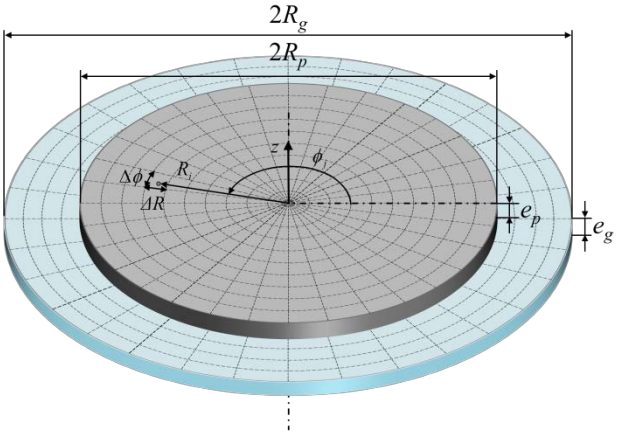

Fig. 3. Discretization grid used in the finite differences method. The grid is based in a polar coordinate system, in which the position of the element i, j is given by R_i and ϕ_j, and ΔR, $\Delta\phi$ are the size of the grid in radial and azimuthal directions.

where N, M are the number of nodes in the grid in radial and azimuthal directions, n is the index of the last element of the disk in radial direction, $T^{\tau}_{p_{i,j}}$ and $T^{\tau}_{g_{i,j}}$ are the temperatures of elements i, j of the disk and the glass in the previous instant. The coefficients $a_p, a^{*}_p, b_p, c_p, d_p$ are different in the boundaries and inside the grid, and are presented in Table 1. The coefficients $a_g, a^{*}_g, b_g, c_g, d_g$ are presented as well in Table 2.

The effect of the radiation increases with the temperature of the material, as seen in (5) and (7). Thus, the value of the losses factor in the disk and the glass is recalculated on each iteration, using the temperature values from the previous instant:

$$h_p = h_{p_{conv}} + h_{p_{rad}} = h_{p_{conv}} + \sigma\varepsilon \left(T^{\tau 2}_p + T^2_a\right)\left(T^{\tau}_p + T_a\right) \quad (15)$$

$$h_g = h_{g_{conv}} + h_{g_{rad}} = h_{g_{conv}} + \sigma\varepsilon\left(T_g^{\tau 2} + T_a^2\right)\left(T_g^{\tau} + T_a\right) \ . \tag{16}$$

The convection coefficients and the contact conductance between the disk and the glass are obtained from experimental results with an induction hob in stationary regime.

Table 1. Coefficients in the equation of the thermal model for the disk, in the case of induction, electric and gas cookers.

Node index	a_{p_i}	$a^*_{p_i}$	$b^+_{p\,i}$	$b^-_{p\,i}$	c_{p_i}	d_{p_i}
$i = 1$	$\frac{\lambda_p}{\Delta R^2} + \frac{\lambda_p}{R_1\,\Delta R} + \frac{2\lambda_p}{R_1^2\,\Delta\phi^2} + \frac{\rho_p\,C_{p_p}}{\Delta t} + \frac{h_p}{e_p} + \frac{h_c}{e_p}$	$\frac{h_p}{e_p}$	$-\left(\frac{\lambda_p}{\Delta R^2} + \frac{\lambda_p}{R_1\,\Delta R}\right)$	0	$-\left(\frac{\lambda_p}{R_1^2\,\Delta\phi^2}\right)$	$\frac{h_c}{e_p}$
$1 < i < n$	$\frac{2\lambda_p}{\Delta R^2} + \frac{\lambda_p}{R_i\,\Delta R} + \frac{2\lambda_p}{R_i^2\,\Delta\phi^2} + \frac{\rho_p\,C_{p_p}}{\Delta t} + \frac{h_p}{e_p} + \frac{h_c}{e_p}$	$\frac{h_p}{e_p}$	$-\left(\frac{\lambda_p}{\Delta R^2} + \frac{\lambda_p}{R_i\,\Delta R}\right)$	$-\left(\frac{\lambda_p}{\Delta R^2}\right)$	$-\left(\frac{\lambda_p}{R_i^2\,\Delta\phi^2}\right)$	$\frac{h_c}{e_p}$
$i = n$	$\frac{\lambda_p}{\Delta R^2} + \frac{2\lambda_p}{R_n^2\,\Delta\phi^2} + \frac{\rho_p\,C_{p_p}}{\Delta t} + \frac{h_p}{e_p} + \frac{h_c}{e_p} + \frac{h_b}{\Delta R} + \frac{h_b}{R_n}$	$\frac{h_p}{e_p} + \frac{h_b}{\Delta R} + \frac{h_b}{R_n}$	0	$-\left(\frac{\lambda_p}{\Delta R^2}\right)$	$-\left(\frac{\lambda_p}{R_n^2\,\Delta\phi^2}\right)$	$\frac{h_c}{e_p}$

Table 2. Coefficients in the equation of the thermal model for the glass, in the case of induction and electric cookers.

Node index	a_{g_i}	$a^*_{g_i}$	$b^+_{g\,i}$	$b^-_{g\,i}$	c_{g_i}	d_{g_i}
$i = 1$	$\frac{\lambda_g}{\Delta R^2} + \frac{\lambda_g}{R_1\,\Delta R} + \frac{2\lambda_g}{R_1^2\,\Delta\phi^2} + \frac{\rho_g\,C_{p_g}}{\Delta t} + \frac{h_c}{e_g}$	0	$-\left(\frac{\lambda_g}{\Delta R^2} + \frac{\lambda_g}{R_1\,\Delta R}\right)$	0	$-\left(\frac{\lambda_g}{R_1^2\,\Delta\phi^2}\right)$	$\frac{h_c}{e_g}$
$1 < i \leq n$	$\frac{2\lambda_g}{\Delta R^2} + \frac{\lambda_g}{R_i\,\Delta R} + \frac{2\lambda_g}{R_i^2\,\Delta\phi^2} + \frac{\rho_g\,C_{p_g}}{\Delta t} + \frac{h_c}{e_g}$	0	$-\left(\frac{\lambda_g}{\Delta R^2} + \frac{\lambda_g}{R_i\,\Delta R}\right)$	$-\left(\frac{\lambda_g}{\Delta R^2}\right)$	$-\left(\frac{\lambda_g}{R_i^2\,\Delta\phi^2}\right)$	$\frac{h_c}{e_g}$
$n < i < N$	$\frac{2\lambda_g}{\Delta R^2} + \frac{\lambda_g}{R_i\,\Delta R} + \frac{2\lambda_g}{R_i^2\,\Delta\phi^2} + \frac{\rho_g\,C_{p_g}}{\Delta t} + \frac{h_g}{e_g}$	$\frac{h_g}{e_g}$	$-\left(\frac{\lambda_g}{\Delta R^2} + \frac{\lambda_g}{R_i\,\Delta R}\right)$	$-\left(\frac{\lambda_g}{\Delta R^2}\right)$	$-\left(\frac{\lambda_g}{R_i^2\,\Delta\phi^2}\right)$	0
$i = N$	$\frac{2\lambda_g}{\Delta R^2} + \frac{\lambda_g}{R_N\,\Delta R} + \frac{2\lambda_g}{R_N^2\,\Delta\phi^2} + \frac{\rho_g\,C_{p_g}}{\Delta t} + \frac{h_g}{e_g}$	$\frac{\lambda_g}{\Delta R^2} + \frac{\lambda_g}{R_N\,\Delta R} + \frac{h_g}{e_g}$	0	$-\left(\frac{\lambda_g}{\Delta R^2}\right)$	$-\left(\frac{\lambda_g}{R_N^2\,\Delta\phi^2}\right)$	0

2.2. Electric stove

In the electric stove (Fig. 4) the power is transferred by radiation from a hot electric resistance to a ceramic glass, which is heated up to temperatures around 400ºC, and transfers the heat to the pan placed on the glass by conduction. The power density distribution depends on the temperature of the resistance T_r with:

$$P = \frac{\sigma \varepsilon}{e_g} \left(T_r^4 - T_g^4\right) . \tag{17}$$

In contrast with the direct heat generation in the pan which occurs in an induction hob, the heating source in the electric stove generates a power distribution in the glass. Hence, the heat flux in vertical direction flows in this case from the glass to the pan. This affects to the boundary condition (9) of the previous model, which is reformulated as:

$$-\lambda_g \left.\frac{\partial T_g}{\partial z}\right|_{z=-e_g} = \sigma \varepsilon \left(T_r^4 - T_g^4\right) = P\, e_g . \tag{18}$$

However, the rest of the boundary conditions are the same as those considered in the model of the induction cooker.

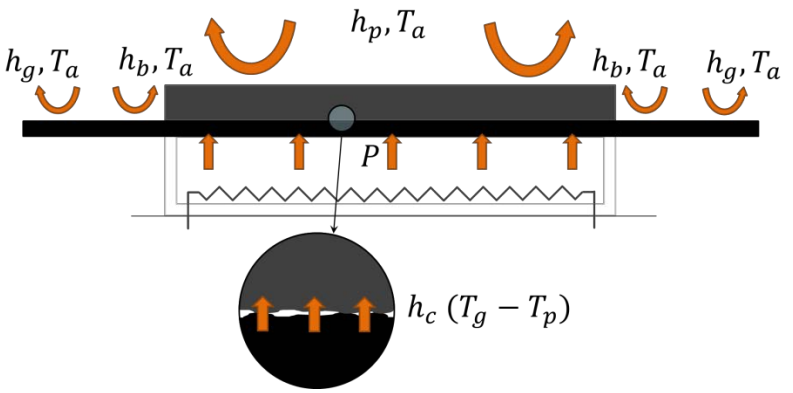

Fig. 4. Scheme of the thermal model in an electric stove. The resistor beneath the glass dissipates electric energy increasing its temperature and radiates heat to the surface of the glass, generating a power distribution P. Heat is transferred to the pan by conduction from the glass, through a contact conductance factor h_c. The losses to the environment from the pan and the glass are modeled with heat transfer coefficients h_p, h_g , which include convection and radiation. The losses in the perimeter of the pan base are modeled with a different heat transfer coefficient h_b.

Using the same numerical method with the discretization grid shown in Fig. 3 the power density distribution $P_{i,j}$ can be obtained with the expresions

$(1 \le i \le n,\ \ 1 \le j \le M)$

$$0 = a_{p_i} T_{p_{i,j}} + b_{p\,i}^{+} T_{p_{i+1,j}} + b_{p\,i}^{-} T_{p_{i-1,j}} + c_{p_i} T_{p_{i,j+1}} + c_{p_i} T_{p_{i,j-1}} - \frac{\rho_p\, C_{p_p}}{\Delta t}\, T_{p\,i,j}^{\tau} - a_{p_i}^{*} T_a - d_{p_i} T_{g_{i,j}} \tag{19}$$

$(1 \le i \le n,\ \ 1 \le j \le M)$

$$P_{i,j} = a_{g_i}\, T_{g_{i,j}} + b_{g}^{+}{}_i\, T_{g_{i+1,j}} + b_{g}^{-}{}_i\, T_{g_{i-1,j}} + c_{g_i}\, T_{g_{i,j+1}} + c_{g_i}\, T_{g_{i,j-1}} - \frac{\rho_g\, C_{p_g}}{\Delta t}\, T_{g}^{\tau}{}_{i,j} - a_{g_i}^{*}\, T_a - d_{g_i} T_{p_{i,j}} \tag{20}$$

$(n < i \leq N,\ \ 1 \leq j \leq M)$

$$P_{i,j} = 0 \tag{21}$$

where it is considered that the disk diameter is equal or larger than the electric resistance diameter. The values of the coefficients are the same as in the induction cooker model, which were presented in Table 1 and Table 2.

2.3. Gas burner

In the gas cooker (Fig. 5) there is a heat exchange between the gas produced in the combustion process and the bottom surface of the pan. The relationship between the configuration of the burner, the flame and the power distribution generated, can be studied with a computational fluid dynamics (CFD) analysis of the problem similar to that carried out in [16], where the heat transfer mechanism is modeled as convection. If we considered a heat transfer coefficient h_{gas} , it would be related to the power density distribution which heats the pan with

$$P = \frac{h_{gas}}{e_p}(T_f - T_p) \tag{22}$$

where T_f is the flame temperature.

The thermal model in this case is simpler, since only the base of the pan is considered and there is no glass between the plate and the heating source. The boundary conditions in radial direction and in the top surface of the plate are the same, and in the bottom surface the heat flux is given by the heat transmission from the flame:

$$-\lambda_p \left.\frac{\partial T_p}{\partial z}\right|_{z=0} = h_{gas}\left(T_f - T_p\right) = P\, e_p\,. \tag{23}$$

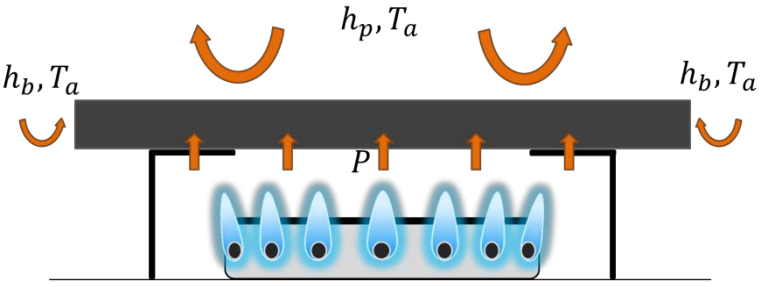

Fig. 5. Scheme of the thermal model in a gas cooker. The combustion gas heats the plate by convection, generating a power distribution P in the base of the pan. The losses to the environment are modeled with a heat transfer coefficient h_p which includes convection and radiation, and the losses in the disk border are modeled with a different heat transfer coefficient h_b.

Again, a numerical calculation method based in finite differences is used. In this case the domain considered only includes the disk. The power distribution in each element $P_{i,j}$ for each instant is obtained with the expression:

$(1 \leq i \leq n,\ \ 1 \leq j \leq M)$

$$P_{i,j} = a_{p_i} T_{p_{i,j}} + b^{+}_{p\,i} T_{p_{i+1,j}} + b^{-}_{p\,i} T_{p_{i-1,j}} + c_{p_i} T_{p_{i,j+1}} + c_{p_i} T_{p_{i,j-1}} - \frac{\rho_p C_{p_p}}{\Delta t} T^{\tau}_{p\,i,j} - a^{*}_{p_i} T_a \quad (24)$$

where the coefficients a, a^*, b, c are the same as presented in Table 1, considering $h_c = 0$.

3. Materials and methods

The model presented in the previous section for an induction hob, an electric stove and a gas cooker requires knowing the temperature on the pan base during a heating process. In order to use the model for the study of real situations, some experiments with real stoves have been carried out, heating ferromagnetic steel disks and measuring the temperatures with an infrared camera.

3.1. Experimental setup

Three conventional cooktops are used to perform the experiments: an induction hob, an electric stove, and a gas cooker, Fig. 6. Different C45 ferromagnetic steel disks of 0.23 m of diameter and thickness from 3e-3 to 5e-3 m, emulating the base of conventional pans, are heated with the three cooktops. The thermal properties of the steel and of the ceramic glass which is present in the induction hob and the electric stove are shown in Table 3. The

186 measurement of the disk temperature has been carried out with an infrared camera FLIR A650 (Fig. 7), which
187 records the temperature evolution at each point with resolution of 640x480 pixels and accuracy of ± 2 ºC.

188 Fig. 6. Cooktops employed in the experiments, one of each type of heating source: induction hob (PIE375N14E), electric stove (3EE721LS) and
189 gas stove (PPQ716B91E).

190 Fig. 7. Infrared camera FLIR A655sc used to measure the temperature distribution.

191 Table 3. Thermal properties of C45 ferromagnetic steel and of the conventional ceramic glass.

Property	Value	Units	Property	Value	Units
λ_p	46	$\frac{\mathrm{W}}{\mathrm{m}\cdot\mathrm{K}}$	λ_g	2.6	$\frac{\mathrm{W}}{\mathrm{m}\cdot\mathrm{K}}$
ρ_p	7850	$\frac{\mathrm{kg}}{\mathrm{m}^3}$	ρ_g	2600	$\frac{\mathrm{kg}}{\mathrm{m}^3}$
C_{p_p}	500	$\frac{\mathrm{J}}{\mathrm{kg}\cdot\mathrm{K}}$	C_{p_g}	800	$\frac{\mathrm{J}}{\mathrm{kg}\cdot\mathrm{K}}$

3.2. Thermography and temperature filtering

The thermographies recorded with the infrared camera in the experiments with the induction hob, the electric stove and the gas cooker, contain on each pixel the mean temperature measured in the corresponding pixel area. This information must be processed before computing the inverse model with two operations: a coordinate transformation and a noise-reduction filtering.

The original image gives the temperature data for each point in a rectangular grid, which must be converted to a polar grid in order to fit the proposed model. For this purpose a coordinate change is performed, using a cubic interpolation algorithm in Matlab. In the resultant image the data in the first row is the temperature in the center of the disk and the last row contains the temperatures in the circumference of the disk border. Thus the radial direction is given along the rows, and the azimuthal direction along the columns (Fig. 8).

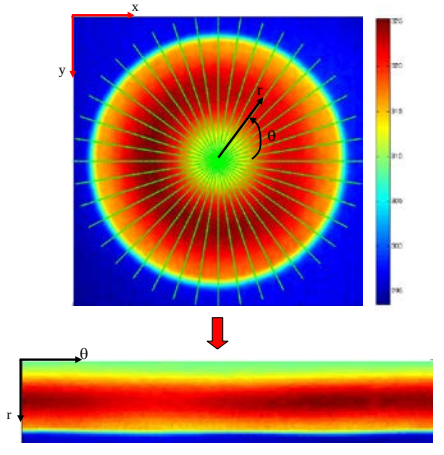

Fig. 8. Coordinates transformation of the thermographies recorded with the infrared camera.

The infrared camera provides the temperature measurement with a certain noise level, which is produced by the non-uniformity of the emissivity of the disk surface and the own signal noise of the infrared sensor. Moreover the discrete nature of the data in the images produces discontinuities in the derivatives after the coordinate transformation. Hence, in order to improve the calculation of temperature derivatives, the images must be filtered in a previous stage. In this work we propose to use a smooth filter proposed by Savitzky & Golay, [17], which is one of the most commonly used filters in image smoothing due to the improved results which can be obtained with respect to other filters such as mean or median filters. An example of the behavior of this filter is shown in Fig. 9, where

both the original and filtered temperature profiles along the disk radius are shown. The first derivative shows the high noise suppression obtained.

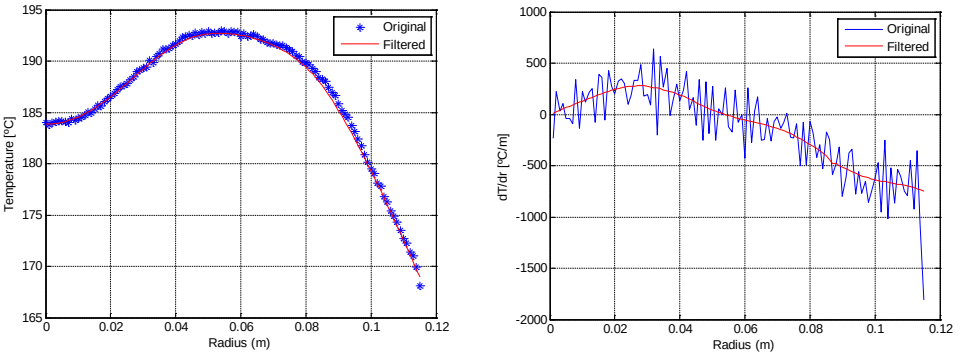

Fig. 9. Smooth filtering with the Savitzky-Golay method. Radial profile and first derivative of the original and filtered data.

3.3. Parameter identification

Although the model takes into account the thermal properties of the materials, which are known from the literature, there have been also considered other parameters such as convection coefficients or the contact conductance, which are specific of each problem. In order to identify these parameters, an experimental procedure is proposed in this section.

In order to simplify the identification of the parameters, it is only used the induction hob because the measurement and control of the input power can be obtained with higher accuracy. A power analyzer (Yokogawa PZ4000) is connected in the output of the power stage which feeds the inductor and the real heating power dissipated in the disk is estimated as the 97% of the power measured, which is the typical efficiency of the inductor [18]. Two different configurations are used in the experiments. First, the glass of 4e-3 m is replaced with an isolation blanket of the same thickness, which simplifies the model and allows considering null heat conduction through the bottom surface of the disk, i.e. the contact conductance is negligible, $h_c = 0$. With the temperatures measured in these experiments the losses coefficients h_p and h_b can be easily identified. Once the values of these parameters are known, from different experiments under the same conditions using the glass instead of the blanket, the contact conductance is obtained.

The C45 steel disks are heated with a low power level, such that the stationary regime is reached at a mean temperature around 250 ºC. Thus, the parameters are calculated by means of the energy balance in the stationary regime, obtained from the measurement of the temperature and the input power. The first balance is obtained by integrating the heat equation in the whole disk, in which both the losses through the top surface and the disk border are taken into account. The resultant expression is

$$P_T - \iint_{0,0}^{R_p,2\pi} h_p\left(T_p - T_a\right) r\, dr\, d\phi - \iint_{0,0}^{e_p,2\pi} h_b\left(T_{p_b} - T_a\right) R_p\, d\phi\, dz = 0 \tag{25}$$

where P_T is the total mean power measured in the coil with the power analyzer, and T_{p_b} is the temperature in the border of the disk. The integral terms are numerically obtained using the same polar grid proposed for solving the theoretical model:

$$\iint_{0,0}^{R_p,2\pi} h_p\left(T_p - T_a\right) r\, dr\, d\phi = \sum_{i,j}^{n,M} \left(h_{p_{conv}}(T_{p_{i,j}} - T_a) + \sigma\varepsilon(T_{p\,i,j}^4 - T_a^4) \right) \frac{(R_i^2 - R_{i-1}^2)\Delta\phi}{2} \tag{26}$$

$$\iint_{0,0}^{e_p,2\pi} h_b\left(T_{p_b} - T_a\right) R_p\, d\phi\, dz = \sum_{j}^{M} \left(h_b(T_{p_{n,j}} - T_a) \right) e_p R_p \Delta\phi \tag{27}$$

The second balance is stated in the disk border, where the boundary condition (11) is employed:

$$\iint_{0,0}^{e_p,2\pi} -\lambda_p \frac{\partial T_{p_b}}{\partial r}\, R_p\, d\phi\, dz = \iint_{0,0}^{e_p,2\pi} h_b\left(T_{p_b} - T_a\right) R_p\, d\phi\, dz \tag{28}$$

The solution of the system with two equations and two unknowns gives the value of h_p and h_b in the considered experiment. In order to obtain a better adjustment, the mean values from several experiments with different input powers have been calculated.

The losses coefficient in the glass surface h_g is obtained experimentally. In this case a round pan with water is placed on the induction hob with the glass beneath, and it is heated up to reach a uniform boiling. Then the induction cooker is switched off and the pan is removed, letting the infrared camera measure the glass temperature. The glass is cooled by effect of the losses coefficient, which can be obtained with an energy balance

$$\int_{t_1}^{t_2}\left(\iint_{0,0}^{R_p,2\pi} h_g\left(T_g - T_a\right) r\, dr\, d\phi + \iint_{0,0}^{e_g,2\pi} -\lambda_g \frac{\partial T_{g_b}}{\partial r}\, R_p\, d\phi\, dz\right) dt = \int_{t_1}^{t_2} \rho_g\, C_{p_g}\, \frac{\partial T_g}{\partial t} dt \tag{29}$$

where $[t_1, t_2]$ is the considered time interval.

Once the losses parameters are identified, the contact heat transfer h_c can be experimentally identified. Using the induction cooktop with a conventional glass, a disk is heated and its temperature recorded with the camera. From a power balance in the disk with the temperature evolution measured, the power transferred from the disk to the glass P_c can be calculated:

$$P_c = P_T - P_{losses} - P_{stored}$$

$$P_c = \iint_{0,0}^{R_p,2\pi} h_c\left(T_p - T_g\right)\, r\, dr\, d\phi$$

$$P_{losses} = \iint_{0,0}^{R_p,2\pi} h_p\left(T_p - T_a\right) r\, dr\, d\phi + \iint_{0,0}^{e_p,2\pi} h_b\left(T_{p_b} - T_a\right) R_p\, d\phi\, dz + \iint_{R_p,0}^{R_g,2\pi} h_g\left(T_g - T_a\right) r\, dr\, d\phi \tag{30}$$

$$P_{stored} = \frac{1}{\Delta t}\int_{t}^{t+\Delta t} \rho_p\, C_{p_p}\, \frac{\partial T_p}{\partial t} dt \ .$$

An example of this calculation is shown in Fig. 10, where each contribution to the power balance is plotted separately. The heated disk has a diameter of 0.23 m and a thickness of 4e-3 m. The coil has a diameter of 0.21 m and the ceramic glass has a thickness of 4e-3 m. The values estimated for the losses coefficients in this case are $h_{p_{conv}} = 9.5 \frac{\mathrm{W}}{\mathrm{m^2K}}$ and $h_b = 75 \frac{\mathrm{W}}{\mathrm{m^2K}}$. In order to obtain the value of the contact conductance the temperature of the glass must be obtained, which at the same time depends on the contact conductance. Thus, an iterative algorithm is used to simulate the temperature of the glass, based on the equations of the theoretical model proposed, for different values of h_c. Then the power transferred from the disk to the glass is calculated from the simulations and compared with the obtained through (30). We select a value of the coefficient with which a best fitting is obtained. For the considered case the calculated value is $h_c = 50 \frac{\mathrm{W}}{\mathrm{m^2K}}$. The fitting between the curves of power transferred from disk to glass is presented in Fig. 11.

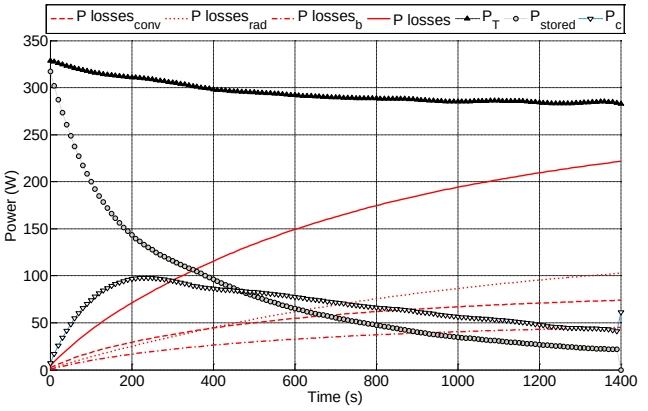

Fig. 10. Power balance obtained from the temperature measurement when heating a disk of diameter 0.23 m and thickness 4e-3 m with a 0.21 m coil in an induction cooktop.

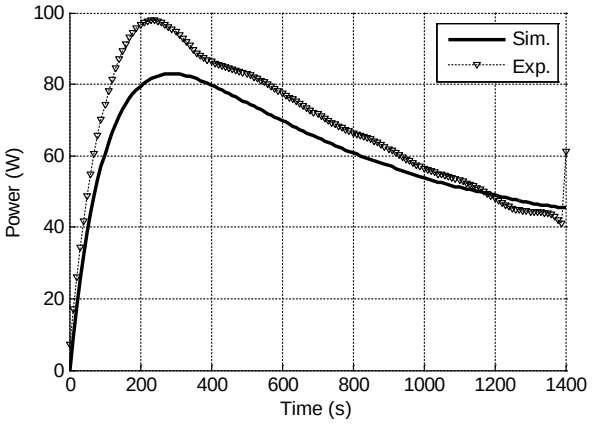

Fig. 11. Power transferred from disk to glass due to the contact conductance with the time. The experimental and simulated curves are shown.

4. Results and discussion

In this section, the power density distribution in different heating situations with the three technologies considered in this work is calculated with the proposed inverse model. The values of the parameters in the model are identified using the previous method with long duration experiments in which a stationary heating is reached. Nevertheless, in order to improve the quality of the results obtained with the inverse model, the power density is obtained from new experiments using higher power levels, considering the transient regime of the heating process.

The larger inductor of the induction hob with two cooking zones is used for heating a disk of 0.23 m of diameter

and 3e-3 m of thickness. The coil diameter is 0.21 m, with a non-equally spaced distribution of turns, as seen in Fig. 12. The power stage which feeds the inductor is a half-bridge resonant inverter, and it is activated with constant frequency and duty cycle during the heating process, which ends when the maximum temperature reached in the disk is 200 ºC. The temperature of the disk is measured with the infrared camera and the power density distribution is calculated for each instant with the proposed inverse model, using the parameters shown in Table 4. An example of the result is presented in Fig. 13, which shows a three-dimensional representation of the power distribution generated in the disk after 20 s, normalized to a total power of 1W. We also present the temperature map in color scale at the same instant. Fig. 14 shows the evolution of the mean power calculated by integration of the power density distribution, and the measured power in the output of the power stage. The result obtained from the model shows a good agreement with the experimental data.

Table 4. Parameter values identified for a disk of 0.23 m of diameter and 0.003 m of thickness, placed on a ceramic glass.

Parameter	Value	Units
$h_{p_{conv}}$	9.5	$\frac{\mathrm{W}}{\mathrm{m^2 \cdot K}}$
h_b	75	$\frac{\mathrm{W}}{\mathrm{m^2 \cdot K}}$
$h_{g_{conv}}$	15	$\frac{\mathrm{W}}{\mathrm{m^2 \cdot K}}$
h_c	50	$\frac{\mathrm{W}}{\mathrm{m^2 \cdot K}}$

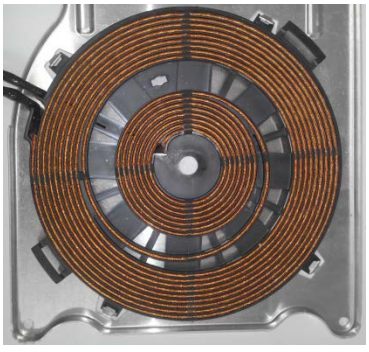

Fig. 12. Planar coil in the conventional induction hob with 0.21 m of diameter and optimized geometry for a uniform heating.

The same disk is heated with the double cooking zone of the electric stove, which consists of two resistances that can be activated independently, Fig. 15. The diameter of the inner resistance is 0.12 m and the diameter of the outer resistance is 0.21 m. The maximum power level of the cooking zone is selected, such that both heating elements are fed constantly from mains with a mean consumption of 1990 W, measured in the input of the stove. The temperature of the disk is measured with the infrared camera and the inverse model is calculated using the same values of the parameters from the previous case. The temperature map in the instant in which the maximum temperature reaches 200 ºC and the 3D representation of the normalized power distribution transmitted from the glass to the disk through the contact conductance are shown in Fig. 16. This power distribution is comparable with the power distribution generated inside the disk in the case of the induction hob, because it is the one which determines the temperature distribution in the pan. Nevertheless the power distribution which heats the glass and the glass temperature can also be obtained with the model. Integrating the power distribution in the disk volume for each instant, the mean power transferred to the disk along the time is obtained, Fig. 17. The difference between this curve and the power measured in the input of the electric hob is the energy employed to heat up the resistance and the glass, which involves spending more than the 60% of the supplied energy.

Finally, a similar experiment is carried out with the gas stove, burning butane gas in the medium-sized burner with a diameter of 0.12 m. The maximum power supplied by this burner is 3000 W, according to the manufacturer, and the gas faucet is opened approximately at the half of the maximum. The temperature of the disk is monitored and the power distribution transferred through the bottom surface of the plate is calculated with the inverse model. The obtained results are presented in Fig. 18. Again, the mean power transferred to the disk for each instant is calculated by integrating the power density distribution in the disk volume, Fig. 19.

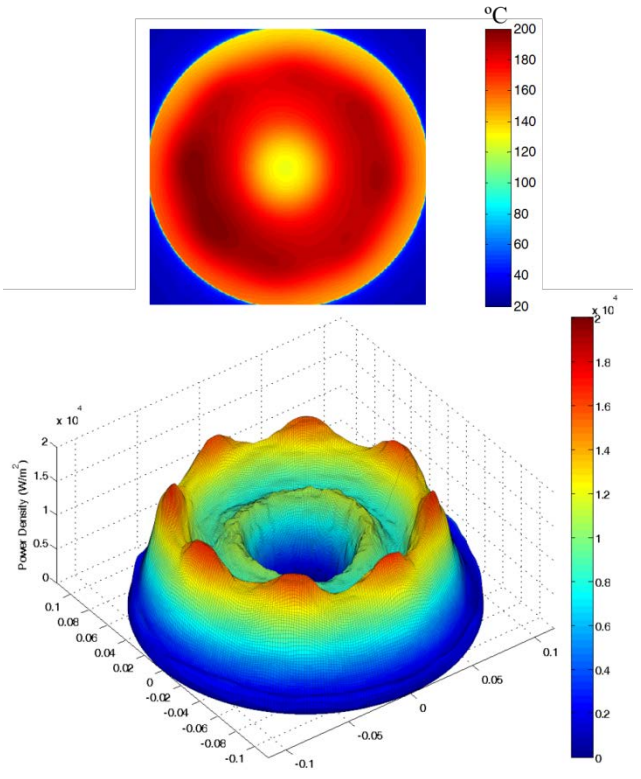

301 Fig. 13. Temperature map measured with the infrared camera and 3D representation of the normalized power density distribution obtained with
302 the inverse model for the inductor of diameter 0.21 m after 20 s of heating.

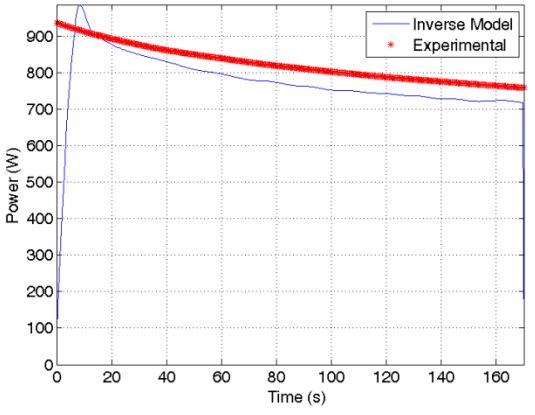

303 Fig. 14. Evolution of the mean power which heats the disk in the induction hob. The measured power and the calculated with the inverse model
304 are in good agreement.

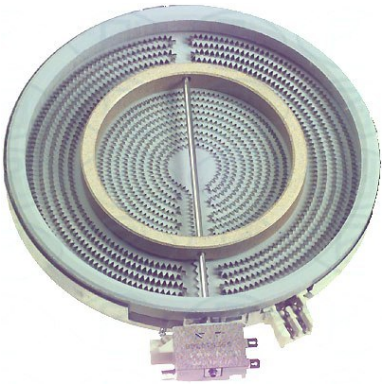

Fig. 15. Double resistance in the electric stove. The inner resistance has a diameter of 0.12 m and the outer resistance a diameter of 0.21 m.

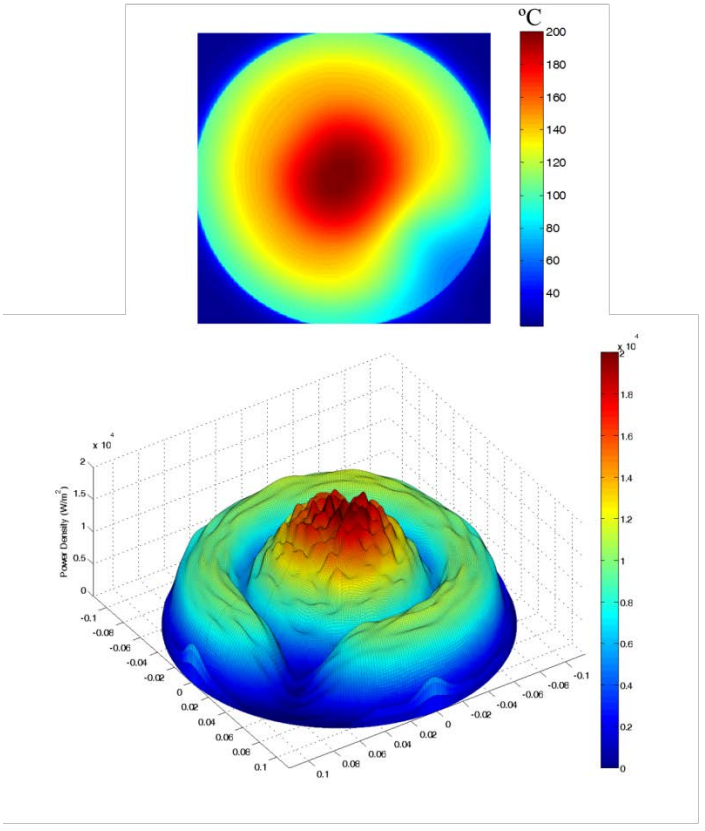

Fig. 16. Temperature map measured with the infrared camera after 125 s of heating and 3D representation of the normalized power density distribution transferred from the glass to the disk calculated with the inverse model for the double cooking zone of the electric stove.

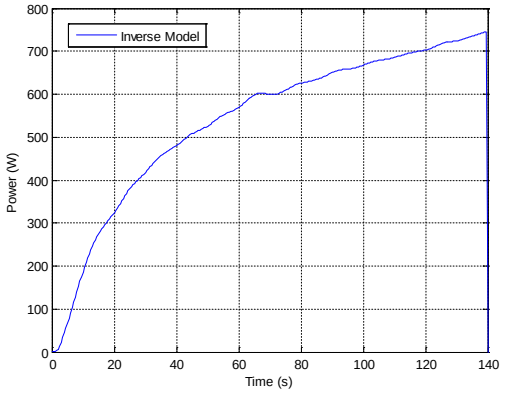

Fig. 17. Evolution of the mean power which heats the disk, transferred through the bottom surface in the electric stove.

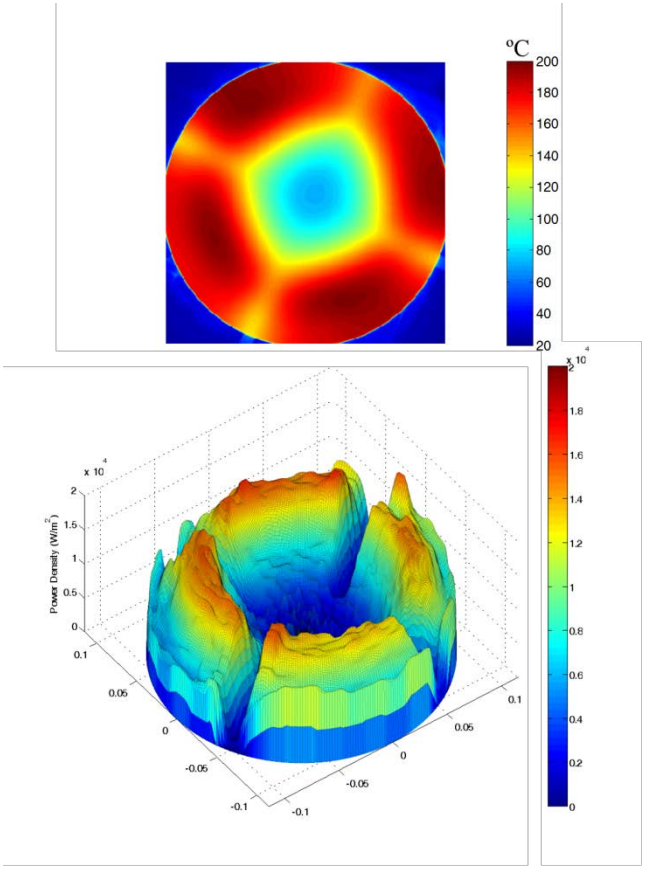

Fig. 18. Temperature map measured with the infrared camera after 72 seconds of heating and 3D representation of the normalized power density distribution, calculated with the inverse model, transferred to the base of the plate from the burnt gas.

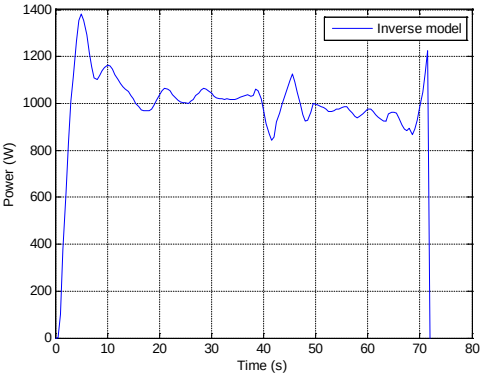

Fig. 19. Evolution of the mean power which heats the disk using the medium-size burner in the gas stove.

From the obtained results, the heating performance of the three considered technologies can be observed and compared. There are some differences in the power distributions which heat the disk, which are a consequence of the type of heating source.

In the case of the induction hob, the power distribution is null in the center of the pan and has two maximums in the radial direction, which are produced by the particular distribution of wire turns of the coil. It is also observed the effect of the 8 ferrite bars beneath the coil, which produce an amplification effect of the magnetic field over its position, increasing the efficiency of the coil. The evolution of the mean power transferred to the disk shows the effect of the temperature in the electrical conductivity of the material, which decreases as the material is heated, thus the induced current decreases and the dissipated power is lower. Nevertheless, in a conventional induction hob the power control implemented in the induction electronics automatically corrects the modulation parameters in order to obtain a constant power supply.

The power distribution transferred to the disk in the double cooking zone of the electric stove shows a peak in the central area of the plate, which is originated by the higher power density radiated by the internal resistance. It can be also observed the effect of the ring which isolates both resistances, producing a low-power area with circular shape. The mean power transferred from the glass to the disk is much lower than the power measured in the input of the stove. This reflects the behavior of this technology in a transient heating, in which the resistance and the glass take the major part of the energy to be heated up to the working temperature. As a result, the efficiency of the stove during the first minutes of a preheating process is low, seen from the point of view of the pan.

The power distribution generated in the gas cooker shows a maximum in the area in which the temperature of the flame is higher, and a large central zone in which the burnt gas has a lower incidence. It can also be observed the effect of the metallic structure which supports the disk above the burner, which isolates the plate surface from the flame and generates gaps in the power distribution. The evolution of the mean power shows in this case that a high power is transferred from the beginning of the heating process, and there is a fluctuation of the power transfer due to the instability of the flame temperature and the gas flow.

5. Conclusions

In this work the thermal modeling in the most common cooking stoves, with different heating technologies, has been presented. The inverse model developed in this paper allows the calculation of the power distribution heating the base of the pan, from the measurement of the temperature distribution with an infrared camera.

The proposed model provides good results with the three considered technologies (induction, electric resistance and gas), and can be used to establish comparisons between the different power distributions and achieve a deeper understanding of the different behavior of the pan temperature during a cooking process in each situation. In the particular cookers studied in this work, the induction hob provides a more uniform power distribution and efficiency when using a cooking vessel of a similar size than the inductor. However, the gas cooker is suitable for a wider range of pan sizes, because the power is more concentrated in the outer area of the pan base. The electric stove showed the worst performance in the heating uniformity, which could be improved by increasing the power supplied by the outer resistance in the double cooker.

The proposed inverse model is an alternative method for the calculation of the power distribution which can be used in situations where a higher computational cost is required with other methods, e.g. with finite element methods or CFD. The results obtained with the inverse model are of high interest and can be employed to simulate heating processes with a direct thermal model in situations under different conditions, with different pans or including the effect of the food.

Acknowledgements

This work has been partially supported by projects IPT-2011-1158-920000 (INNPACTO) and RTC-2014-

1847-6 (RETOS-COLABORACION), from Ministerio de Economia y Competitividad, Spain, and by grant AP2013/02769 from Ministerio de Educacion, Cultura y Deporte, Spain.

References

[1] J. Cernela, B. Heyd, B. Broyart, Evaluation of heating performances and associated variability of domestic cooking appliances (oven-baking and pan-frying), Appl. Therm. Eng. 62 (2014) 758–765. doi:10.1016/j.applthermaleng.2013.08.045.

[2] F.J. Cadavid, Y. Cadavid, A.A. Amell, A.E. Arrieta, J.D. Echavarría, Numerical and experimental methodology to measure the thermal efficiency of pots on electrical stoves, Energy. 73 (2014) 258–263. doi:10.1016/j.energy.2014.06.017.

[3] S.E. Zorrilla, R.P. Singh, Heat transfer in double-sided cooking of meat patties considering two-dimensional geometry and radial shrinkage, J. Food Eng. 57 (2003) 57–65. doi:10.1016/S0260-8774(02)00273-X.

[4] A.H. Feyissa, K. V. Gernaey, S. Ashokkumar, J. Adler-Nissen, Modelling of coupled heat and mass transfer during a contact baking process, J. Food Eng. 106 (2011) 228–235. doi:10.1016/j.jfoodeng.2011.05.014.

[5] F. Sanz, C. Sagues, S. Llorente, Induction Heating Appliance with a Mobile Double-Coil Inductor, IEEE Trans. Ind. Appl. 51 (2015) 1945–1952. doi:10.1109/TIA.2014.2367136.

[6] J.K. Byun, K. Choi, H.S. Roh, S.Y. Hahn, Optimal design procedure for a practical induction heating cooker, IEEE Trans. Magn. 36 (2000) 1386–1389. doi:10.1109/20.877697.

[7] H.N. Pham, H. Fujita, K. Ozaki, N. Uchida, Estimating Method of Heat Distribution Using 3-D Resistance Matrix for Zone-Control Induction Heating Systems, IEEE Trans. Power Electron. 27 (2012) 3374–3382. doi:10.1109/TPEL.2011.2179984.

[8] M. Souley, J. Egalon, S. Caux, O. Pateau, Y. Lefevre, P. Maussion, Optimization of the settings of multiphase induction heating system, IEEE Trans. Ind. Appl. 49 (2013) 2444–2450. doi:10.1109/TIA.2013.2264924.

[9] P. Wikström, W. Blasiak, F. Berntsson, Estimation of the transient surface temperature and heat flux of a steel slab using an inverse method, Appl. Therm. Eng. 27 (2007) 2463–2472. doi:10.1016/j.applthermaleng.2007.02.005.

[10] F.L. Rodríguez, V. De Paulo Nicolau, Inverse heat transfer approach for IR image reconstruction: Application to thermal non-destructive evaluation, Appl. Therm. Eng. 33-34 (2012) 109–118. doi:10.1016/j.applthermaleng.2011.09.019.

[11] A. Plotkowski, M. Krane, The Use of Inverse Heat Conduction Models for Estimation of Transient Surface Heat Flux in Electroslag Remelting, J. Heat Transfer. 137 (2015) 031301–031301–9. doi:10.1115/1.4029038.

[12] J. Luo, A.J. Shih, Inverse Heat Transfer Solution of the Heat Flux Due to Induction Heating, J. Manuf. Sci. Eng. 127 (2005) 555–563. doi:10.1115/1.1949617.

[13] J. Zhou, Y. Zhang, J.K. Chen, Z.C. Feng, Inverse estimation of surface heating condition in a three-dimensional object using conjugate gradient method, Int. J. Heat Mass Transf. 53 (2010) 2643–2654. doi:10.1016/j.ijheatmasstransfer.2010.02.048.

[14] T.L. Bergman, A.S. Lavine, F.P. Incropera, D.P. Dewitt, Fundamentals of heat and mass transfer, seventh ed, John Wiley & Sons, 2011.

[15] R. LeVeque, Finite Difference Methods for Ordinary and Partial Differential Equations: Steady-State and Time-Dependent Problems, Society for Industrial and Applied Mathematics, 2007. doi:10.1137/1.9780898717839.

[16] J.G. Shin, J.H. Woo, Analysis of Heat Transfer Between the Gas Torch and the Plate For the Application of Line Heating, J. Manuf. Sci. Eng. 125 (2003) 794–800. doi:10.1115/1.1616949.

[17] A. Savitzky, M.J.E. Golay, Smoothing and Differentiation of Data by Simplified Least Squares Procedures, Anal. Chem. 36 (1964) 1627–1639. doi:10.1021/ac60214a047.

[18] J. Acero, J.M. Burdio, L.A. Barragan, D. Navarro, R. Alonso, J.R. García, et al., Domestic induction appliances, IEEE Trans. Ind. Appl. Mag. 16 (2010) 39–47. doi:10.1109/MIAS.2009.935495.